Technical Document 2086
April 1991

Issues and Methods of Broadband Array Processing

M. Reuter

NAVAL OCEAN SYSTEMS CENTER

San Diego, California 92152-5000

J. D. FONTANA, CAPT, USN
Commander

H. R. TALKINGTON, Acting
Technical Director

ADMINISTRATIVE INFORMATION

This work was performed by the Signal Processing Technology Branch, Code 733, Naval Ocean Systems Center (NOSC), under NOSC Block Programs.

Released by
D. K. Barbour, Head
Signal Processing
Technology Branch

Under authority of
J. A. Roese, Head
Signal and Information
Processing Division

JG

CONTENTS

FIGURES

1.0 BROADBAND PROCESSING ISSUES

In this section, we introduce issues related to the analysis of broadband processes in the context of the source localization problem via spatial sampling. We will present a linear systems model of the propagation environment and show how it influences the spatial/spectral estimation of these processes. We also show how this linear systems view lends itself to the analysis of the moving source problem.

1.1 NOTATION

In this document, bold lower case and upper case letters denote vectors and matrices respectively. $\boldsymbol{x}$ represents a vertical vector, $\boldsymbol{x}^H$ its complex conjugate or Hermitian transpose, and $\boldsymbol{x}^T$ its transpose.

1.2 LINEAR SYSTEMS MODEL OF PROPAGATION ENVIRONMENT

Assume that an acoustic source emits a real, zero mean, wide sense stationary (WSS) ergodic random process $s(t)$ with bandwidth B. The process propagates through some acoustic environment, and we spatially sample the field with an array of M sensors. Each sensor is indexed by its location vector $\boldsymbol{\beta}_{si} = (r_{si}, z_{si}, \theta_{si})$ where r_{si}, z_{si}, and θ_{si} denote range, depth, and azimuth with respect to the source. $x(t;\boldsymbol{\beta}_{si})$ represents the process received by the i^{th} sensor due to $s(t)$.

1.2.1 Time-Invariant Channel Filter Model

It is instructive to view $x(t;\boldsymbol{\beta}_{si})$ as resulting from a linear filtering operation on $s(t)$ (Knight, Pridham, and Kay, 1981). Figure 1-1 represents the propagation environment as a bank of linear filters where $h(t;\boldsymbol{\beta}_{si})$ is the time invariant *channel impulse response* for the i^{th} source/sensor-pair filter and $y_i(t)$ is the output of the sensor due to $x(t;\boldsymbol{\beta}_{si})$ and additive noise $n_i(t)$, which is also WSS ergodic and statistically uncorrelated with $x(t;\boldsymbol{\beta}_{si})$. Naturally, these "spatial filters" are causal and stable. We also will assume that the channel bandwidths are much greater than B. Figure 1-2 depicts a sample time invariant impulse response. We can imagine sending an impulse down a channel and receiving this response. Here the time spread $L_i - D_i$ generally can be interpreted as the result of multipath (Kennedy and Lebow, 1964).

If $\sigma_s^2(\omega)$ is the power spectral density of the process $s(t)$, we know that the power spectral density of $x(t;\boldsymbol{\beta}_{si})$ is

$$\sigma^2_{x_{\beta si} x_{\beta si}}(\omega) = |H(\omega;\boldsymbol{\beta}_{si})|^2 \sigma_s^2(\omega) \tag{1.1}$$

and the cross power spectral density of $x(t;\boldsymbol{\beta}_{si})$ and $x(t;\boldsymbol{\beta}_{sk})$ is

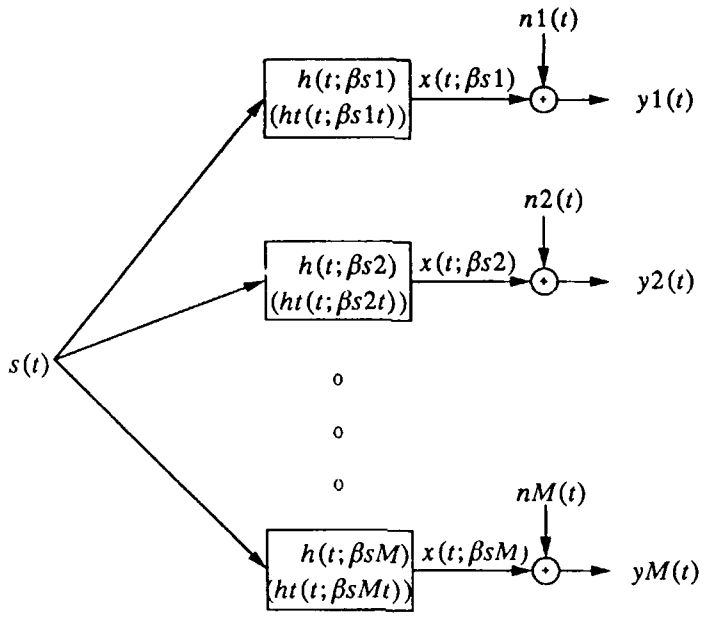

Figure 1-1. Linear systems model of propagation environment.

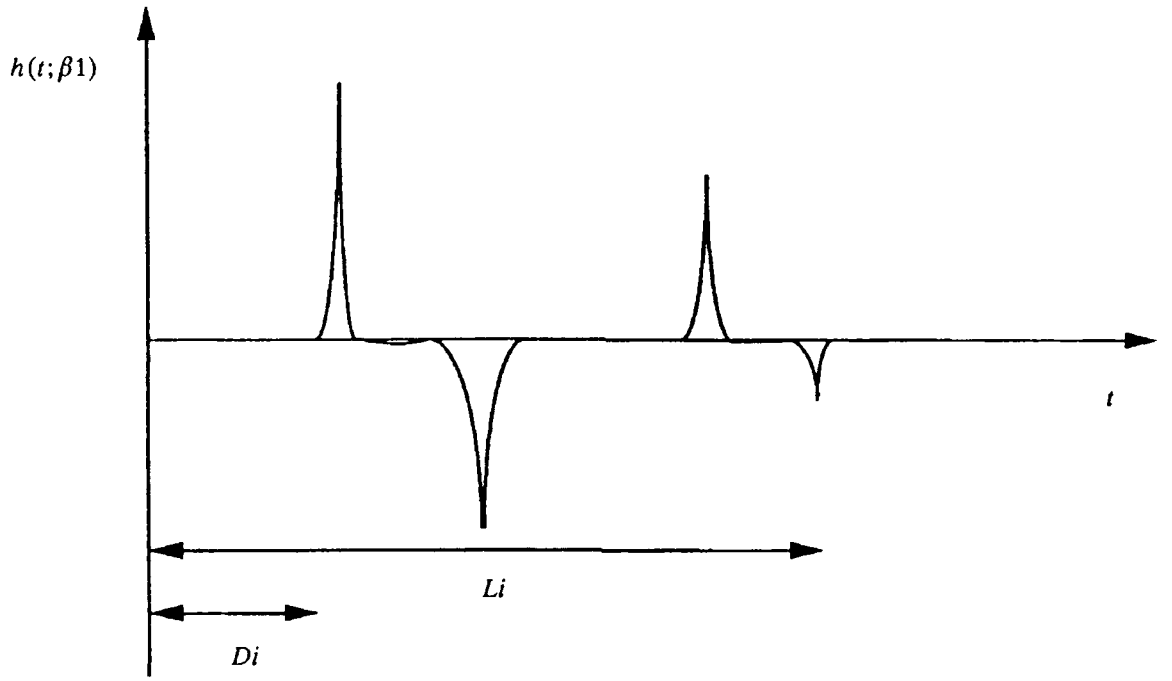

Figure 1-2. Impulse response of i^{th} source/sensor-pair time invariant, causal filter with total length L_i, and initial delay D_i.

$$\sigma^2_{x_{\beta_{si}} x_{\beta_{sk}}}(\omega) = H(\omega;\boldsymbol{\beta}_{si}) H^*(\omega;\boldsymbol{\beta}_{sk}) \sigma^2_s(\omega) \tag{1.2}$$

where $H(\omega;\boldsymbol{\beta}_{si})$ and $H(\omega;\boldsymbol{\beta}_{sk})$ are the frequency responses of the i^{th} and k^{th} source/sensor-pair filters respectively.

1.2.1.1 Array Processing

We first will be concerned with frequency-domain array processing applications (Dudgeon and Mersereau, 1984, and Gingras, 1989) since most well-developed acoustic propagation codes directly compute the channel frequency responses rather than impulse responses. We estimate the temporal/spatial spectrum $P(\omega;\boldsymbol{\beta})$ of the field by computing the quadratic

$$P_{\text{conv}}(\omega;\boldsymbol{\beta}) = \frac{1}{M^2} \boldsymbol{e}^H_{(\omega;\beta)} \boldsymbol{R}(\omega) \boldsymbol{e}_{(\omega;\beta)} \tag{1.3}$$

for the conventional case and

$$P_{\text{mvdr}}(\omega;\boldsymbol{\beta}) = \frac{1}{\boldsymbol{e}^H_{(\omega;\beta)} \boldsymbol{R}^{-1}(\omega) \boldsymbol{e}_{(\omega;\beta)}} \tag{1.4}$$

for the minimum variance distortionless response (MVDR) processor. Here $\boldsymbol{e}_{(\omega;\beta)}$ is the steering vector where the i^{th} element is an estimate of the channel frequency response sampled at ω for the i^{th} sensor indexed by some spatial vector $\boldsymbol{\beta}_i$ (indicating the "look" direction) and $\boldsymbol{R}(\omega)$ is the cross spectral density matrix (CSDM), defined by

$$\boldsymbol{R}(\omega) = \lim_{T \to \infty} \frac{1}{T} E\{\mathbf{y}(\omega)\mathbf{y}^H(\omega)\} \tag{1.5}$$

where the i^{th} element of $\mathbf{y}(\omega)$ is given by the stochastic integral

$$y_i(\omega) = \int_{-T/2}^{T/2} y_i(t) e^{-j\omega t} dt \tag{1.6}$$

and $E\{\ \}$ denotes the expectation operator. For the case of figure 1-1 and using equations 1.1 and 1.2, $\boldsymbol{R}(\omega)$ can be written as

$$\boldsymbol{R}(\omega) = \sigma^2_s(\omega) \boldsymbol{h}_{(\omega;\beta_s)} \boldsymbol{h}^H_{(\omega;\beta_s)} + \boldsymbol{Q}(\omega) \ . \tag{1.7}$$

We refer to $\boldsymbol{h}_{(\omega;\beta_s)}$ as the signal vector where the i^{th} element is $H(\omega;\boldsymbol{\beta}_{si})$ and $\boldsymbol{Q}(\omega)$ represents the CSDM of the noise process $n_i(t)$. We compute equations 1.3 or 1.4 for various $(\omega;\boldsymbol{\beta})$, and if $\boldsymbol{e}_{(\omega;\beta)} = \dfrac{\boldsymbol{h}_{(\omega;\beta_s)}}{\left|\boldsymbol{h}_{(\omega;\beta_s)}\right|}$ we will get a peak on the $(\omega,\boldsymbol{\beta})$ surface.

1.2.1.2 Plane-Wave Case

The above analysis also applies to the well-known plane-wave-based array processing problem. In this case, the impulse responses of figure 1-1 will be delta functions shifted in

time t by an amount corresponding to the direct path delay. For the case in figure 1-2, $h(t;\boldsymbol{\beta}_i)$ would be equal to $\delta(t - D)$ and the elements of $\boldsymbol{h}(\omega;\boldsymbol{\beta}_s)$ would be the corresponding phase shifts.

1.2.1.3 Estimating the CSDM

We know that since $s(t)$ is WSS and ergodic and $h(t;\boldsymbol{\beta}_{si})$ is stable and time invariant, $x(t;\boldsymbol{\beta}_{si})$ and $y(t_i)$ also are WSS ergodic. So the ensemble average of equation 1.5 can be estimated using frequency averages by dividing the sensor data into K *sufficiently long segments* and computing

$$\hat{\boldsymbol{R}}(\omega) = \frac{1}{K}\sum_{\ell=1}^{K} \mathbf{y}_\ell(\omega)\mathbf{y}_\ell^H(\omega) \tag{1.8}$$

where $\mathbf{y}_\ell(\omega)$ is calculated from the normalized Fourier transform of the l^{th} segment of data (Johnson, 1982). Generally, as K and the respective transform length become larger and the time gap between the l^{th} and the $(l - 1)^{th}$ Fourier transforms becomes smaller, $\hat{\boldsymbol{R}}(\omega)$ becomes a "better" estimate of $\boldsymbol{R}(\omega)$. Usually $K > M$.

1.2.1.4 Fourier Transform Length/Spectral Sampling Rate

The method of estimating the CSDM from equation 1.8 requires us to compute Fourier transforms that are "sufficiently long." Aside from the statistical requirements needed to estimate the source power spectral density ($\sigma_s^2(\omega)$ in equation 1.7), the necessary length must be a function of the array geometry and the propagation environment. To see this let $s(t)$ be a broadband process and let

$$\begin{aligned} x_{li}(\omega) &= \frac{1}{\sqrt{T_f}} \int_{t_\ell}^{t_\ell + T_f} \int_{D_i}^{L_i} s(t-\tau)\, h(\tau;\boldsymbol{\beta}_{si})\, e^{-j\omega t} d\tau\, dt \\ &= \frac{1}{\sqrt{T_f}} \int_{D_i}^{L_i} h(\tau;\boldsymbol{\beta}_{si}) \int_{t_\ell}^{t_\ell + T_f} s(t-\tau)\, e^{-j\omega t} d\tau\, dt \end{aligned} \tag{1.9}$$

be the signal component of the i^{th} element of the l^{th} vector from equation 1.8. Now, if

$$\dot{S}_l(\omega) = \frac{1}{\sqrt{T_f}} \int_{t_\ell}^{t_\ell + T_f} s(t)\, e^{-j\omega t}\, dt \tag{1.10}$$

then

$$x_{li}(\omega) \approx \dot{S}_l(\omega) \int_{D_i}^{L_i} h(\tau;\boldsymbol{\beta}_{si})\, e^{-j\omega\tau} d\tau \tag{1.11}$$

if $T_f >> L_i$. Then

$$x_{li}(\omega) \approx \hat{S}_l(\omega)\, H(\omega;\boldsymbol{\beta}_{si}) \,. \tag{1.12}$$

Now, since we really are interested in correlations *between* sensors, i.e., phase differences between elements of $\boldsymbol{x}_l$ (ω) as in equation 1.2, the condition that $T_f >> L_i$ might be too strict. We can imagine time-shifting the impulse responses of the source/sensor pair filters by an amount $D_s = \min(D_1,D_2,\ldots,D_M)$. Then if $L_s = \max(L_1,L_2,\ldots,L_M)$, we can approximate good phase differences for all sensor pair elements of the CSDM if

$$T_f >> L_s - D_s \,. \tag{1.13}$$

This result is analogous to the plane-wave case where the length of the Fourier transform is required to be much longer than the maximum propagation time across the array (Wax, Shan, and Kailath, 1984).

Interestingly, this requirement is less important for narrowband processes (Wax, Shan, and Kailath, 1984) and, in fact, is unnecessary for sinusoidal processes. To see this, assume $s(t)$ is a complex sinusoidal process $e^{j(\omega_0 t+\phi)}$ where ϕ is some random phase. Then equation 1.10 becomes

$$\begin{aligned} \hat{S}_l(\omega) &= \frac{e^{j\phi}}{\sqrt{T_f}} \int_{t_l}^{t_l+T_f} e^{-j(\omega-\omega_0)t}\, dt \\ &= c\ \mathrm{sinc}\left[(\omega-\omega)\frac{T_f}{2}\right] \end{aligned} \tag{1.14}$$

where c is a complex constant. Then equation 1.11 becomes

$$x_{li}(\omega) = \hat{S}_l(\omega) \int_{D_i}^{L_i} h(\tau;\boldsymbol{\beta}_{si}) e^{-j\omega_0\tau} d\tau \tag{1.15}$$

regardless of the size of T_f .

We know that given a certain *temporal sampling rate*, T_f will determine the frequency sampling rate or discrete Fourier transform (DFT) binwidth, i.e.,

$$\Delta\omega = \frac{2\pi}{T_f} \tag{1.16}$$

for ω in radians/second. So we can see that the acoustic propagation environment (characterized by L_s and D_s) will dictate the maximum coarseness of the $(\omega,\boldsymbol{\beta})$ search space and as a result influence our calculation of the steering vectors of equations 1.3 and 1.4.

1.2.1.5 Broadband Definition

Analogous with the definitions given in Wax, Shan, and Kailath (1984) and Hudson (1981), we *define* a source to be *narrowband* with respect to some array/source configuration if

$$B << \frac{1}{L_s - D_s}, \tag{1.17}$$

where L_s and D_s are from section 1.2.1.4. It is *broadband* otherwise.

1.2.2 Time-Variant Channel Filter Model

Realistically, however, the channel filters rarely are time invariant (we have included the time-variant impulse responses in the ( )s in figure 1.1). There might be random perturbations in the channel caused by moving scatterers, moving sea surface, or a moving source (Knight, Pridham, and Kay, 1981). In this case, $x(t;\beta_{si})$ and $y_i(t)$ will not be WSS (Weinstein, 1978) since $x(t;\beta_{si})$ will not be the linear convolution of $s(t)$ and $h(t;\beta_{si})$ and so the concept of a CSDM then has no meaning. To deal with this situation, we usually assume that a segment of data is a windowed portion of WSS data and we try to estimate the statistics of this "imaginary" data using the segment as in equation 1.8. The more slowly varying the filters, the longer we can make the window and the better our estimates get.

Problems can result when K in equation 1.8 is large compared to the time-varying nature of the propagation environment. Usually a lack of coherence between sensors results, which manifests itself in the calculation of $\hat{R}(\omega)$, e.g., for the environment of figure 1-1 we will not get the cross sensor statistics of equation 1.2. Usually for large arrays and long-source ranges, the random channel perturbations cause this lack of coherence (Morgan and Smith, 1990). For shorter ranges, the moving source becomes the primary cause (Gerlach, 1978, and Patzewitsch and Srinath, 1978). In this case, we would expect a certain degree of performance degradation from the spatial processors of equations 1.3 and 1.4 resulting in a loss of output signal-to-noise ratio (SNR), an increase in peak location variance, or bias etc. Indeed if the time-varying nature of the channel is very severe, we might not be able to do any spatial spectral estimation via the methods of equations 1.3, 1.4, and 1.8.

However, attempts have been made at using this time-varying nature as a target discriminant, e.g., the moving source situation in Weinstein (1978). Viewing the problem as in figure 1-1 might allow us also to use time-variant-filter theory for source localization (Chen, 1984, and Kitagawa and Gersch, 1985).

1.3 CORRELATION BETWEEN FOURIER COEFFICIENTS

In our calculations of the CSDM, we only have determined correlations between Fourier coefficients of the same frequency. Since the signal has some frequency extent,

one might wonder if there are correlations between Fourier coefficients that we might use to enhance array processing performance. It can be shown (Papoulis, 1984; Blachman, 1957; and Hodgkiss and Nolte, 1976) that if we define $x_i(\omega_m)$ and $x_k(\omega_n)$ as in equation 1.6 (without the noise component), then

$$\lim_{T \to \infty} \frac{1}{T} E\{x_i(\omega_m)\, x_k^*(\omega_n)\} = 0 \qquad \forall\, i, k, \text{ and } m \neq n \tag{1.18}$$

where m and n are frequency indexes. That is, the "cross-frequency" power spectrum of a WSS process is zero, i.e., the Fourier coefficients at different frequencies are uncorrelated. However, these coefficients in fact are correlated for finite T. An expression of the correlation easily can be derived using equation 1.2 and equation 1.6 (Blachman, 1957, and Hodgkiss and Nolte, 1976) giving

$$\begin{aligned} E\{x_i(\omega_m)x_k^*(\omega_n\} &= \int_{-\frac{T}{2}}^{\frac{T}{2}} \int_{-\frac{T}{2}}^{\frac{T}{2}} r_{x_{ik}}(t-s)\, e^{-j\omega_m t}\, e^{j\omega_n s} dt\, ds \\ &= \frac{T^2}{2\pi} \int_{-\infty}^{\infty} \sigma^2_{x_{\beta si} x_{\beta sk}}(\omega) \text{sinc}\left[\frac{(\omega-\omega_m)T}{2}\right] sinc\left[\frac{(\omega-\omega_n)T}{2}\right] d\omega \end{aligned} \tag{1.19}$$

where $r_{x_{ik}}(t-s)$ is the cross correlation function of the i^{th} and k^{th} processes. We can see that equation 1.19 approaches equation 1.18 when $T \to \infty$ for $m \neq n$ and approaches equation 1.5 for $m = n$.

The conclusions reached in Hodgkiss and Nolte (1976) indicate that if $\sigma^2_{x_{\beta si} x_{\beta sk}}(\omega)$ is fairly constant over the interval where $\text{sinc}\left[\frac{(\omega-\omega_m)T}{2}\right]\text{sinc}\left[\frac{(\omega-\omega_n)T}{2}\right]$ has appreciable value, then equation 1.19 approximates the correlation value for $T \to \infty$. This result is useful for certain frequency-domain array processing implementations (Hodgkiss, 1979). Since this assumption obviously is dependent on the propagation environment, it is unclear how applicable it is to non-plane-wave conditions. A certain degree of correlation actually might enhance array processing performance if used correctly, e.g., in a "cross-frequency" power spectral density matrix.

1.3.1 Frequency Averaging

Interestingly, frequency averaging as in equation 1.8 appears to be a faulty method of estimating equation 1.19. To see this, we define the continuous frequency average as

$$E_{fa}\{x_i(\omega_m)\, x_k^*(\omega_n)\} = \lim_{A \to \infty} \frac{1}{2A} \int_{-A}^{A} x_{it_0}(\omega_m)\, x_{kt_0}^*(\omega_n) dt_0 \tag{1.20}$$

where

$$x_{it0}(\omega_m) = \int_{-\frac{T}{2}+t_0}^{\frac{T}{2}+t_0} x_i(\epsilon)\, e^{-j\omega_m \epsilon} d\epsilon \qquad (1.21)$$

and

$$x^*_{kt_0}(\omega_n) = \int_{-\frac{T}{2}+t_0}^{\frac{T}{2}+t_0} x_k(\alpha)\, e^{j\omega n\alpha} d\alpha \ . \qquad (1.22)$$

Then

$$E_{fa}\{x_i(\omega_m)x_k^*(\omega_n)\} = \lim_{A\to\infty} \frac{1}{2A} \int_{-A}^{A} \int_{-\frac{T}{2}}^{\frac{T}{2}} \int_{-\frac{T}{2}}^{\frac{T}{2}} x_i(t+t_0)x_k(s+t_0)e^{-jt_0(\omega_m-\omega_n)}e^{-j\omega_m t}\, e^{j\omega_n s} dt\, ds\, dt_0 \qquad (1.23)$$

where $t = \epsilon - t_0$ and $s = \alpha - t_0$. Interchanging the order of integration, we get

$$E_{fa}\{x_i(\omega_m)x_k^*(\omega_n)\} = \int_{-\frac{T}{2}}^{\frac{T}{2}} \int_{-\frac{T}{2}}^{\frac{T}{2}} \lim_{A\to\infty} \frac{1}{2A} \int_{-A}^{A} [x_i(t+t_0)x_k(s+t_0)e^{-jt_0(\omega_m-\omega_n)}]dt_0\, e^{-j\omega_m t} e^{j\omega_n s} dt\, ds \ . \qquad (1.24)$$

Now if, $\omega_m = \omega_n$ and using the ergodicity property of $x_{i,k}(t)$, i.e.,

$$\lim_{A\to\infty} \frac{1}{2A} \int_{-A}^{A} x_i(t+t_0)x_k(s+t_0)dt_0 = r_{x_{ik}}(t-s) \ , \qquad (1.25)$$

we get

$$E_{fa}\{x_i(\omega_m)x_k^*(\omega_n)\} = \int_{-\frac{T}{2}}^{\frac{T}{2}} \int_{-\frac{T}{2}}^{\frac{T}{2}} r_{x_{ik}}(t-s)\, e^{-j\omega(t-s)} dt\, ds \ . \qquad (1.26)$$

Then (Thomas, 1984)

$$\lim_{T\to\infty} \frac{1}{T} E_{fa}\{x_i(\omega_m)x_k^*(\omega_n)\} = \lim_{T\to\infty} \frac{1}{T} E\{x_i(\omega_m)x_k^*(\omega_n)\} = \sigma^2_{x_{\beta si}x_{\beta sk}}(\omega) \ . \qquad (1.27)$$

This is the familiar result from section 1.2.1.3. Now if, $\omega_m \neq \omega_n$, we want to arrive at equation 1.19. However, in general

$$\lim_{A \to \infty} \frac{1}{2A} \int_{-A}^{A} x_i(t+t_0)x_k(s+t_0)e^{-jt_0(\omega_m-\omega_n)}dt_0 \neq r_{x_{ik}}(t-s) \ . \tag{1.28}$$

This is easy to see since $r_{x_{ik}}(t - s)$ is real and equation 1.28 is a windowed Fourier transform of $x_i(t + t_0)x_k(s + t_0)$ over the frequency variable $\omega_m - \omega_n$. Since $x_i(t + t_0)x_k(s + t_0)$ is not necessarily an even function, the left side of equation 1.28 in general is complex.

So it appears that frequency averaging cannot be used to estimate correlation between Fourier coefficients at different frequencies. Equation 1.19 indicates one approach is to take a two-dimensional Fourier transform of an estimate of the correlation function.

2.0 METHODS OF BROADBAND ARRAY PROCESSING

In this section, we introduce approaches to recently developed broadband array processing that take advantage of the frequency extent of the source process to estimate its spatial spectrum. The frequency-domain methods essentially collapse a region of the frequency axis from the $(\omega,\boldsymbol{\beta})$ search space and then search over the $(\boldsymbol{\beta})$ region, while the time-domain methods use the linear systems model of the propagation environment to determine matched filters for the spatial search space. Mainly, we will be concerned with MVDR processing.

2.1 BROADBAND MODEL

We use the following standard model of the cross spectral density matrix of equation

$$\boldsymbol{R}(\omega) = \boldsymbol{A}(\omega)\, \boldsymbol{P}_s(\omega)\, \boldsymbol{A}^H(\omega) + \boldsymbol{Q}(\omega) \quad . \tag{2.1}$$

If there are N sources, then $\boldsymbol{A}(\omega)$ is an $M \times N$ matrix whose columns are the signal vectors of the sources. $\boldsymbol{P}_s(\omega)$ is an $N \times N$ matrix whose diagonal elements are the power spectral densities of each source and off-diagonal elements are the respective cross-source spectral densities. If the sources are mutually uncorrelated, $\boldsymbol{P}_s(\omega)$ is a diagonal matrix. $\boldsymbol{Q}(\omega)$ is the noise matrix.

2.2 INCOHERENT FREQUENCY-DOMAIN ARRAY PROCESSING

The simplest and most common approach to broadband array processing is to decompose the process(es) received at the sensors into narrowband components via the Fourier transform, estimate the spatial spectrum using equations 1.3, 1.4, and 1.5, and then *incoherently* sum up the spectrums across the frequency range of interest (Tolstoy and Porter, 1986), i.e.,

$$P_{i\_\mathrm{conv}}(\boldsymbol{\beta}) = \sum_i P_{\mathrm{conv}}(\omega_i;\boldsymbol{\beta}) \tag{2.2}$$

or

$$P_{i\_\mathrm{mvdr}}(\boldsymbol{\beta}) = \sum_i P_{\mathrm{mvdr}}(\omega_i;\boldsymbol{\beta}) \quad . \tag{2.3}$$

The success of this method rests on the fact that spurious peaks resulting from sidelobes incoherently add across frequency, while actual peaks resulting from the sources coherently add. Thus, we might be able to effectively process broadband signals with arrays whose "half-wavelength" sensor spacing is much greater than the wavelengths associated with the spectral composition of the broadband process. This allows us to use sparse arrays and still avoid, to a certain extent, spatial aliasing.

2.2.1 Simulations

Initially, our simulations consist of two mutually uncorrelated sources impinging upon a 16-element line array with 7.5-meter sensor spacing, i.e., the half wavelength spacing for 100 Hz assuming 1500 meter/second sound speed. Both sources are plane waves with 0° declination angle. Source 1 emanates from 180° azimuth and source 2 from 186° azimuth, where 180° represents broadside. Both sources are bandpass, Gaussian processes with bandwidth B = 40 Hz with 100-Hz center frequency. We also include sensor noise (temporally and spatially uncorrelated). The power spectral density values of the source and noise processes are 0 dB within the 80- to 120-Hz band. We note that the sources are plane waves for convenience only and the results given here are applicable to more general propagation environments.

We spectrally decomposed the data into 0.934-Hz binwidths and constructed the narrowband CSDMs with 56 independent fast Fourier transforms (FFTs), which comprised approximately 1 minute of data. Figures 2-1 and 2-2 are the results of the narrowband MVDR processor for 100 Hz and 120 Hz respectively for 10 runs, where each run represents an estimate of the spatial spectrum of the signal and noise processes for some sample function. For both frequencies we see the variance in the array response in the direction of the signals and most notably in the nonsignal directions. This variance is due to inaccuracies in estimating the CSDM.

We get the results shown in figures 2-3 and 2-4 by incoherently summing the array responses across the 80- to 120-Hz frequency range, as in equations 2.2 and 2.3 respectively, for the 10 independent runs. We first note that the conventional processor does not quite resolve the two sources, while the MVDR processor clearly does. We also see a dramatic decrease in MVDR array response variance over the results shown in figures 2-1 and 2-2. Certainly one of the advantages of incoherent processing might be the enhanced detection of low-SNR broadband signals in the presence of strong narrowband or broadband interferers by this decrease in variance of the side regions of the array response.

2.3 COHERENT FREQUENCY-DOMAIN ARRAY PROCESSING

Many methods have been proposed recently that attempt to effectively use the broadband nature of the source to enhance array processing performance (Wang and Kaveh, 1985; Krolik and Swingler, 1989; Buckley, 1987; Buckley and Griffiths, 1988; and Nawab, Dowla, and Lacoss, 1985). Here we will concentrate on the MVDR-based broadband method presented in Krolik and Swingler (1989), which is essentially derived from the approach given in Wang and Kaveh (1985). In this method, the narrowband CSDMs are estimated as in the incoherent technique of section 2.2. Then they are *presteered* to some direction of look and *coherently* summed across the desired spectrum. The resulting steered matrix is then used in an MVDR algorithm.

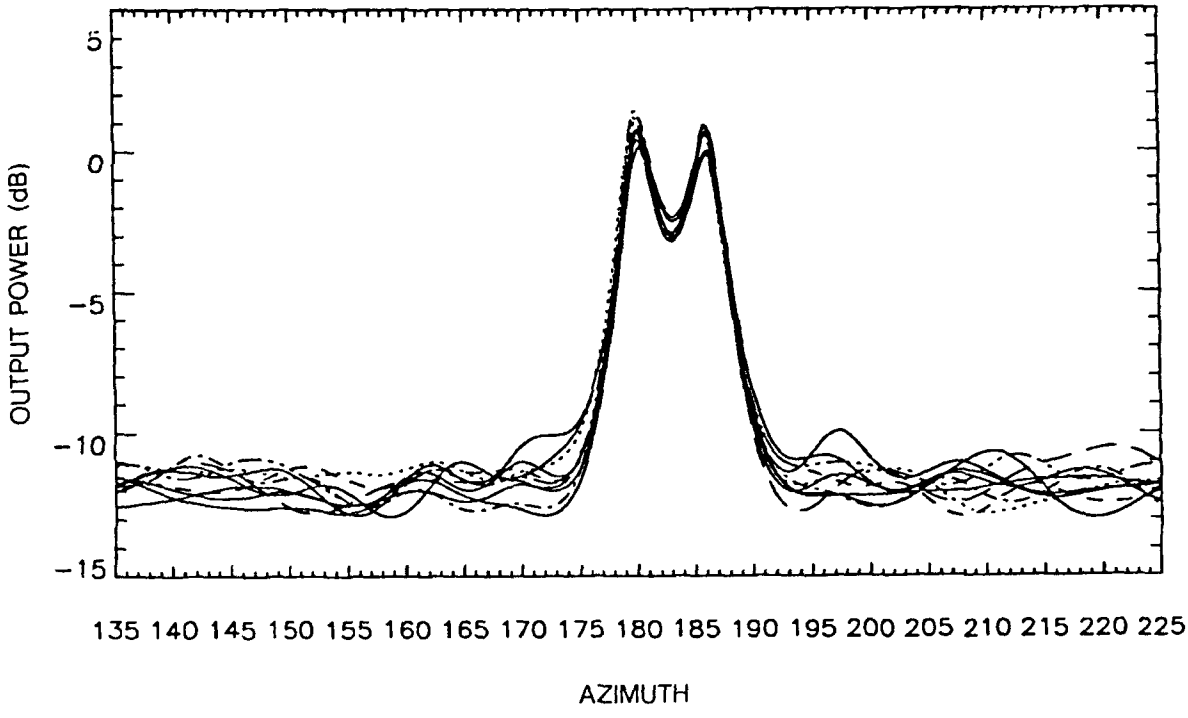

Figure 2-1. Narrowband MVDR processor results at 100 Hz with 56 independent FFTs per CSDM.

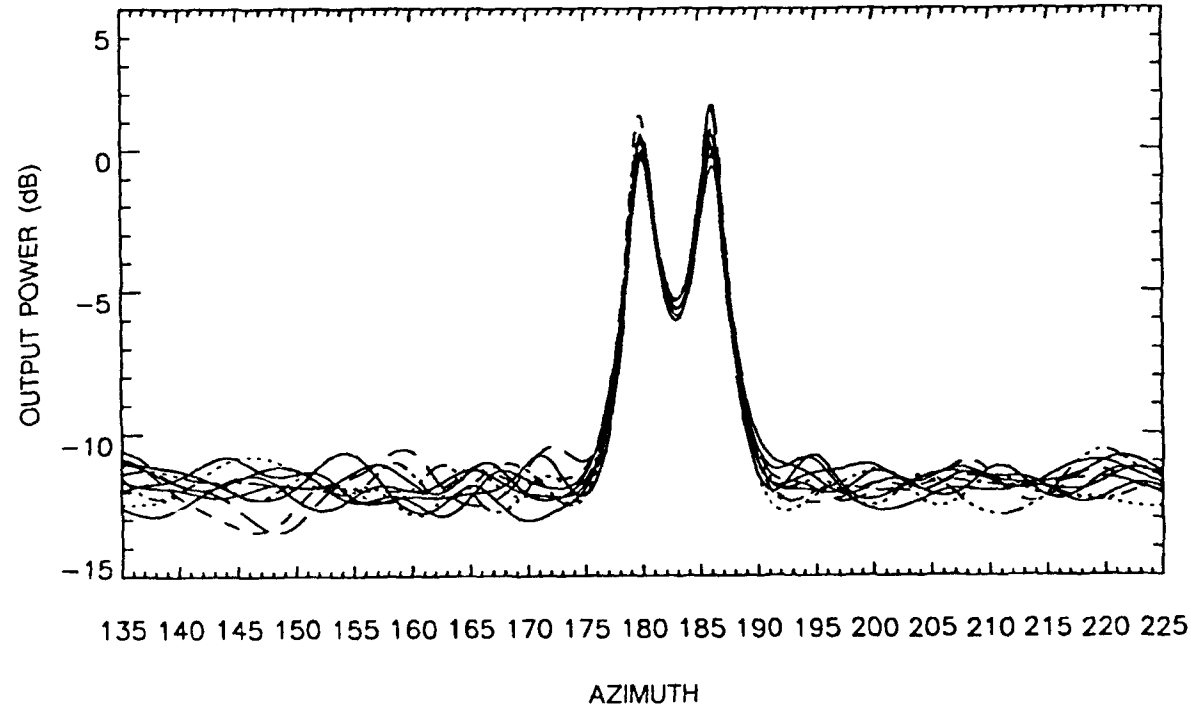

Figure 2-2. Narrowband MVDR processor results at 120 Hz with 56 independent FFTs per CSDM.

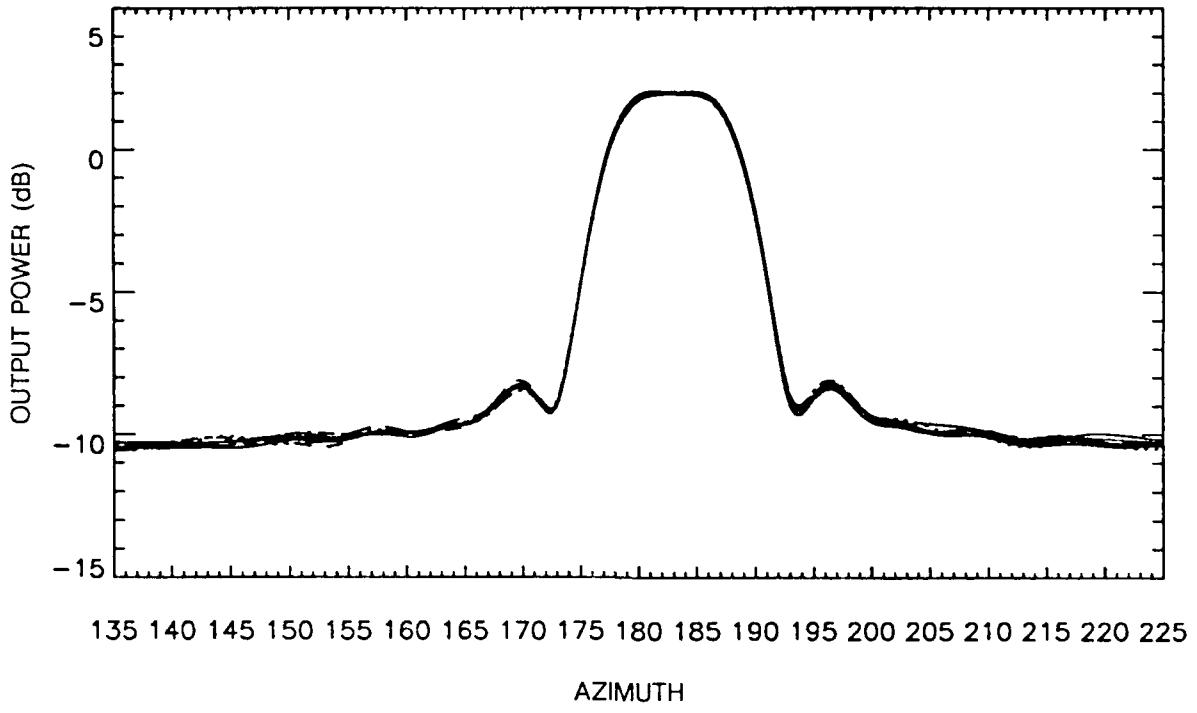

Figure 2-3. Incoherent conventional processor results with 56 independent FFTs per CSDM.

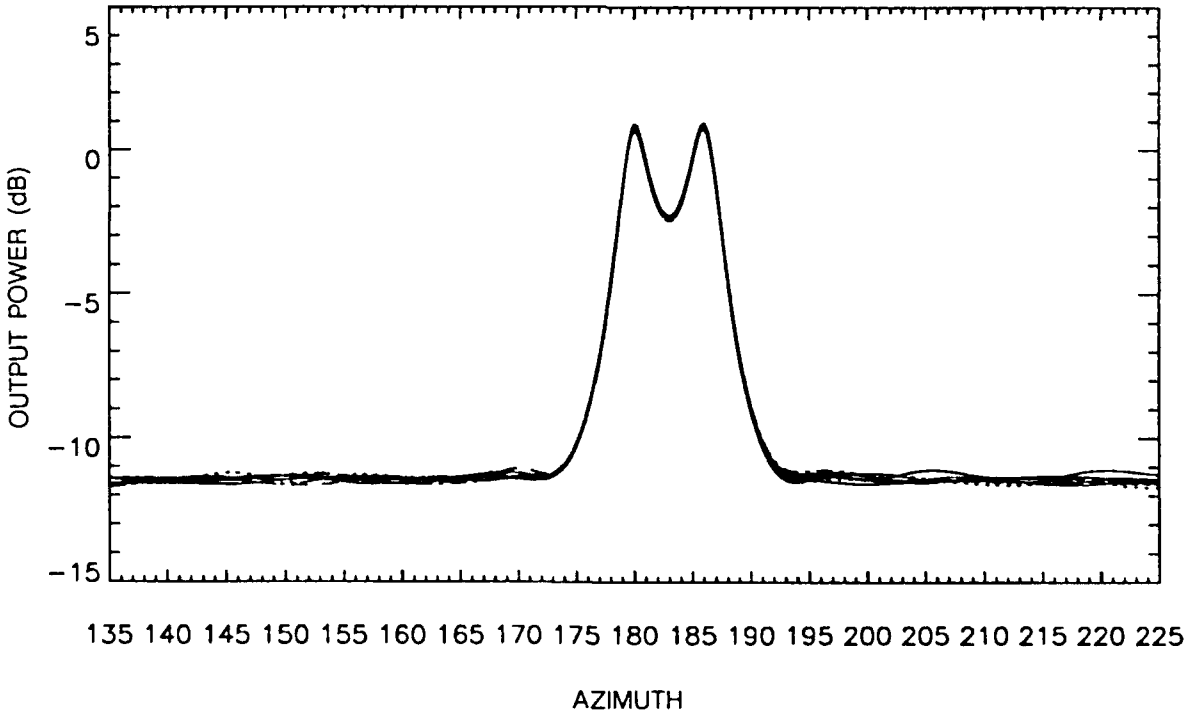

Figure 2-4. Incoherent MVDR processor results with 56 independent FFTs per CSDM.

To begin, we expand equation 2.2 using equation 1.3, i.e.,

$$P_{i\_conv}(\boldsymbol{\beta}) = \frac{1}{M^2} \sum_i \boldsymbol{e}^H(\omega_i;\boldsymbol{\beta})\boldsymbol{R}(\omega_i)\boldsymbol{e}(\omega_i;\boldsymbol{\beta}) \ . \tag{2.4}$$

Now,

$$\boldsymbol{e}(\omega_i;\boldsymbol{\beta}) = \boldsymbol{E}(\omega_i;\boldsymbol{\beta})\mathbf{1} \ , \tag{2.5}$$

where $\boldsymbol{E}(\omega_i;\boldsymbol{\beta})$ is the diagonal matrix

$$\boldsymbol{E}(\omega_i;\boldsymbol{\beta}) = \begin{bmatrix} e_1(\omega_i;\boldsymbol{\beta}) & & & \\ & e_2(\omega_i;\boldsymbol{\beta}) & & 0 \\ & & \cdots & \\ 0 & & & e_M(\omega_i;\boldsymbol{\beta}) \end{bmatrix} \tag{2.6}$$

and $\mathbf{1}$ is an $M \times 1$ vector of ones. So,

$$P_{i\_conv}(\boldsymbol{\beta}) = \frac{1}{M^2}\mathbf{1}^T\left[\sum_i \boldsymbol{E}^H(\omega_i;\boldsymbol{\beta})\boldsymbol{R}(\omega_i)\boldsymbol{E}(\omega_i;\boldsymbol{\beta})\right]\mathbf{1} \ , \tag{2.7}$$

or

$$P_{i\_conv}(\boldsymbol{\beta}) = \frac{1}{M^2}\mathbf{1}^T\left[\sum_i \boldsymbol{R}_{st}(\omega_i;\boldsymbol{\beta})\right]\mathbf{1} \ , \tag{2.8}$$

where $\boldsymbol{R}_{st}(\omega_i;\boldsymbol{\beta})$ is the "steered" CSDM (SCSDM). We can see that if the signal vector of some source described by a column of $\boldsymbol{A}(\omega_i)$ of equation 2.1 is modeled by $\boldsymbol{e}(\omega_i;\boldsymbol{\beta})$, then this signal is mapped onto the $\mathbf{1}$ vector in the operation of equation 2.7. Then, these "mapped" components of the broadband signal are *coherently* added across frequency in equation 2.8 while the other sources represented in $\boldsymbol{A}(\omega_i)$ and the noise components of $\boldsymbol{Q}(\omega_i)$ are *incoherently* summed.

Now, recognizing the similarity between equation 2.8 and equation 1.3, we can see that an MVDR-based method or *coherent* MVDR technique that uses the SCSDMs results in

$$P_{c\_mvdr}(\boldsymbol{\beta}) = \frac{1}{\mathbf{1}^T\left[\sum_i \boldsymbol{R}_{st}(\omega_i;\boldsymbol{\beta})\right]^{-1}\mathbf{1}} \ . \tag{2.9}$$

We note that the interpretation of equation 2.2 given by equation 2.8 implies that $P_{i\_conv}(\boldsymbol{\beta}) = P_{c\_conv}(\boldsymbol{\beta})$ while it is obvious that $P_{c\_mvdr}(\boldsymbol{\beta})$ is markedly different from $P_{i\_mvdr}(\boldsymbol{\beta})$. We define $\sum_i \boldsymbol{R}_{st}(\omega_i;\boldsymbol{\beta})$ as the coherent CSDM or $\boldsymbol{R}_c(\boldsymbol{\beta})$. Then

$$P_{c\_mvdr}(\beta) = \frac{1}{\mathbf{1}^T \mathbf{R}_c^{-1}(\beta)\mathbf{1}} \quad . \tag{2.10}$$

An obvious drawback of the method described by equation 2.9 is that SCSDMs must be estimated, summed, and inverted *for each direction of look*. This might be a considerable computational burden for large arrays. However, the main benefit of this method over the incoherent technique of equation 2.3 is that there are more statistical degrees of freedom available to estimate $\mathbf{R}_c(\beta)$ than are required to estimate each narrowband CSDM (Krolik and Swingler, 1989). So, given some Fourier transform length, we might be able to estimate a "statistically sufficient" $\mathbf{R}_c(\beta)$ using *fewer* Fourier transform updates than the number required to estimate the narrowband CSDMs. This would be of value in highly nonstationary environments as described in section 1.2.2. Also, coherent MVDR easily can be implemented in a parallel processing environment since the coherent CSDMs for all directions of look can be constructed and inverted independently of one another.

We also note that an appropriate steering matrix for broadband coherent MVDR matched-field array processing might be one whose elements are *inverses* of the respective channel frequency response values rather than simply conjugates as described in section 1.0. For plane-wave processing, these two cases are identical.

2.3.1 Simulations

We now analyze the synthetic broadband data described in section 2.2.1 using the coherent broadband MVDR technique of equation 2.9. Spectrally decomposing the data as before, we get the results of figure 2-5 using 56 independent FFTs per CSDM. We note the similarity between figure 2-5 and the incoherent MVDR results of figure 2-4. We can conclude that nothing is gained from the increased computational expense of coherent MVDR if enough data are available to compute well-conditioned narrowband CSDMs (Giannella and Schultheiss, 1990).

Next, we construct the matrices using only *one* outer product or approximately 1 *second* of data. Technically, these matrices are not CSDM estimates since no frequency averaging is done. Since the number of frequency bins is much greater than 16, $\mathbf{R}_c(\beta)$ is full rank and we get the results shown in figure 2-6. We note the considerable increase in variance of the power in the side regions as well as in the direction of the two signals. We also see an increase in peak bias in these two directions. However, both signals are still well localized. Figures 2-7 and 2-8 represent results for two and three FFTs per "CSDM" respectively. We see the gradual decrease in variance and peak bias. In fact, the results of figure 2-8 appear similar in quality to the 100-Hz narrowband result of figure 2-1. There are no incoherent MVDR results that we can compare to figures 2-6, 2-7, and 2-8 since the narrowband CSDMs are singular in these cases.

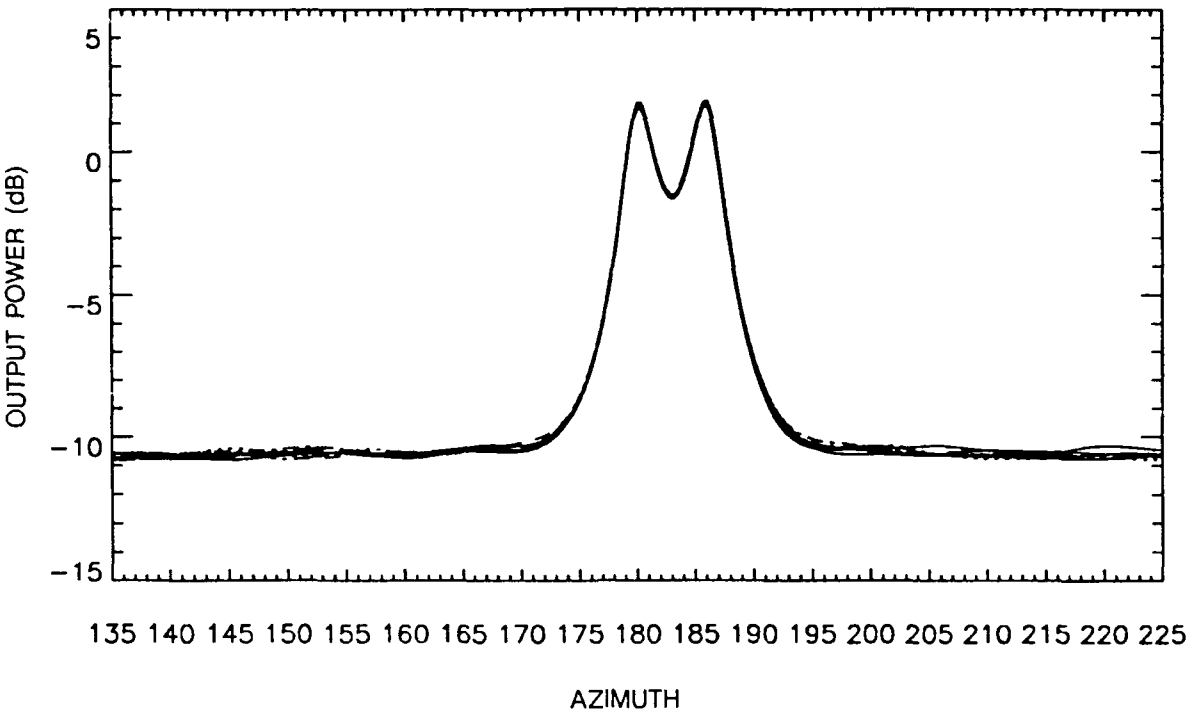

Figure 2-5. Coherent MVDR processor results with 56 independent FFTs per CSDM.

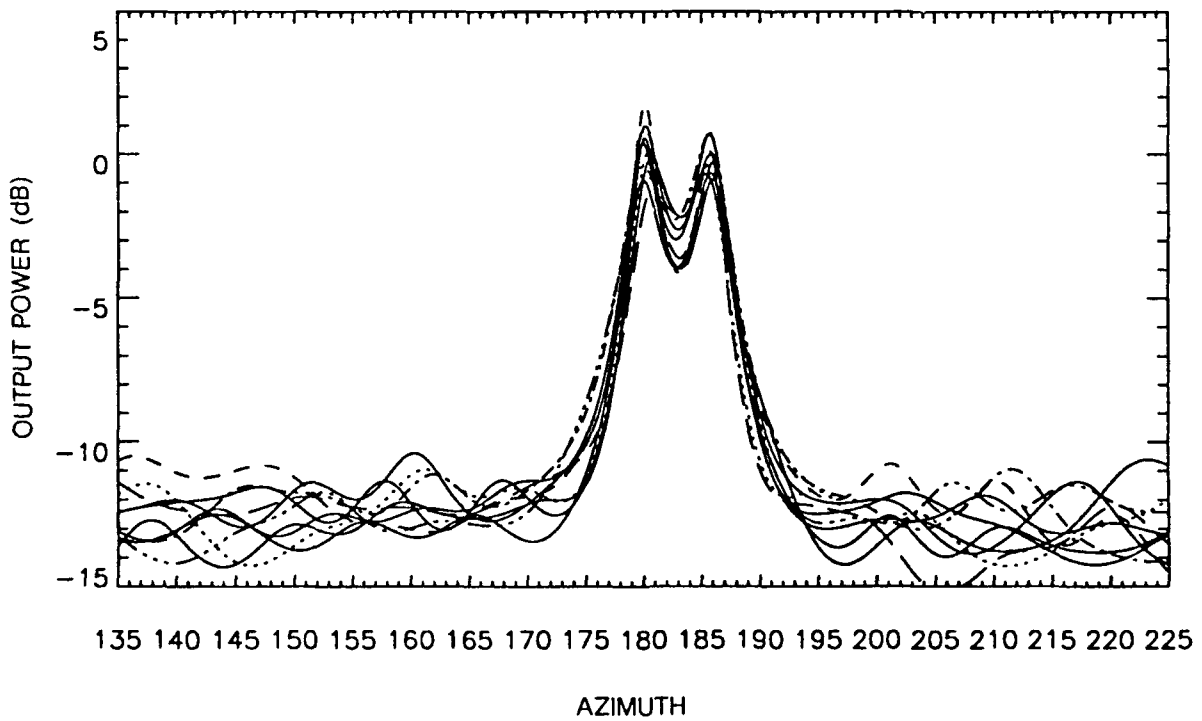

Figure 2-6. Coherent MVDR processor results with one FFT per "CSDM."

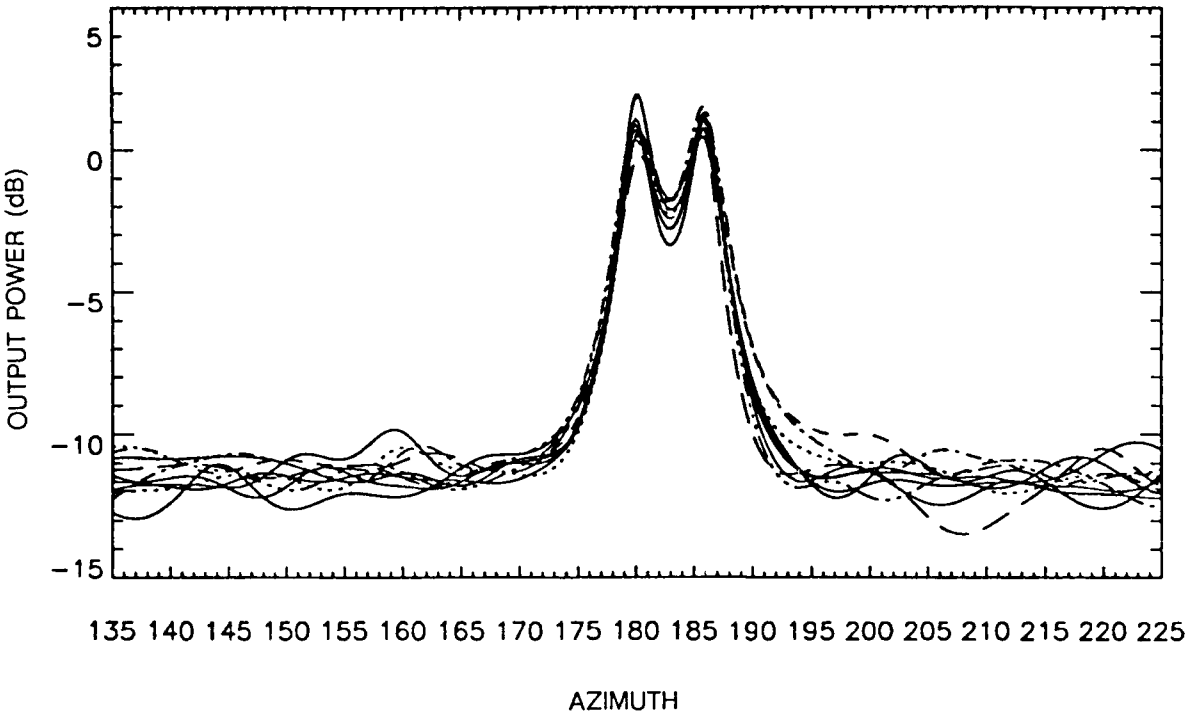

Figure 2-7. Coherent MVDR processor results with two independent FFTs per "CSDM."

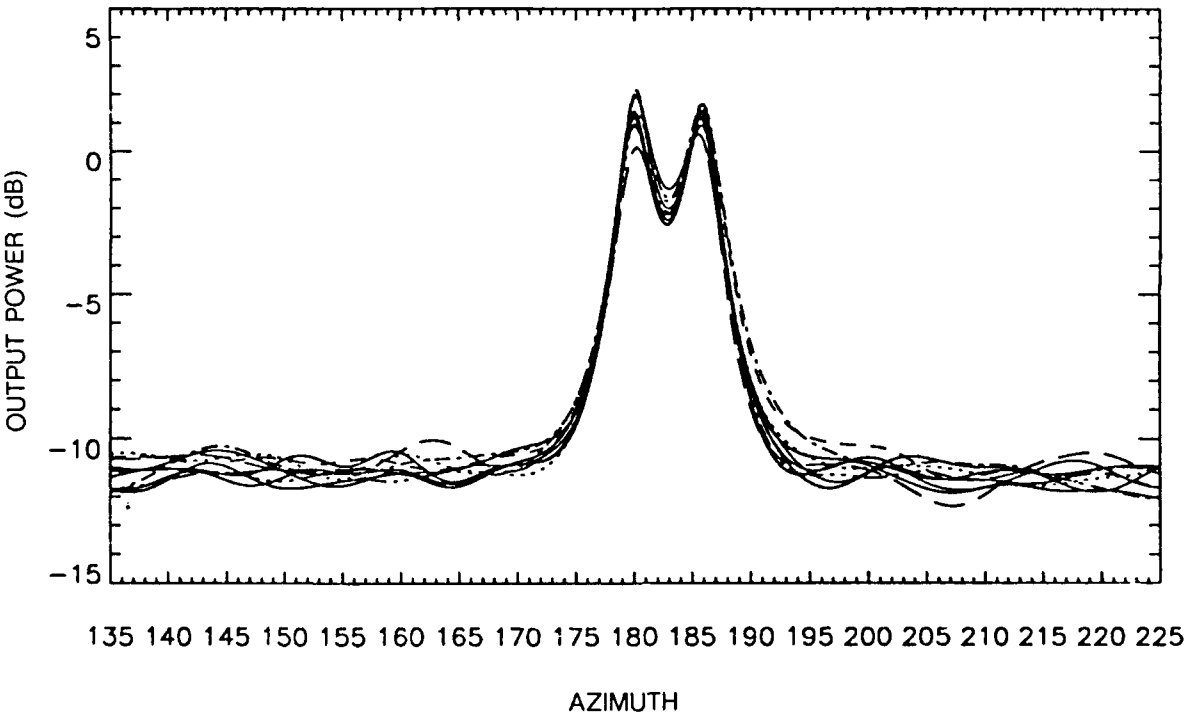

Figure 2-8. Coherent MVDR processor results with three independent FFTs per "CSDM."

2.3.2 Correlated Sources

An additional interesting aspect of the coherent MVDR algorithm is that it is able to localize completely correlated broadband sources as long as the signal vectors are not equal or simple scaler multiples of one another. This is essentially due to the fact that presteering and frequency averaging results in coherent addition only for sources modeled by the steering matrix $\boldsymbol{E}(\omega_i;\boldsymbol{\beta})$ regardless of the power spectral density of the source. The greater the spectral extent of the averaging, the better the performance. See Wang and Kaveh (1985) for a more general explanation.

2.3.2.1 Simulations

For simulation purposes we modify the source characteristics of section 2.2.1 so that the two sources are completely correlated. Figure 2-9 is the result of incoherent MVDR for this case. Interestingly, two sources are apparently detected. However this is due to the fact that, because of the regularity of the array, the resulting correlated signal vector (the sum of the two individual signal vectors) has two prominent sidelobes in these directions. Note that there is considerable peak bias for all the trials. Conversely, figure 2-10 results from coherent MVDR. While there is a considerable drop in output power, there is no significant peak bias.

2.3.3 Multiple Presteering

The coherent MVDR method requires a matrix inverse for each direction of look since the narrowband CSDMs are presteered to only one direction. A modification of this technique would presteer for multiple look directions.

Let $\boldsymbol{B}(\omega_i)$ be an $M \times P$ matrix where each of the P columns is a steering vector representing some direction of look. We want to find a steering matrix $T_{st}(\omega_i;\boldsymbol{B}(\omega_i))$ such that

$$\boldsymbol{T}_{st}(\omega_i;\boldsymbol{B}(\omega_i))\boldsymbol{B}(\omega_i) = \boldsymbol{G}, \tag{2.11}$$

where $\boldsymbol{G}$ is an $M \times P$ matrix whose columns represent vectors upon which we want the respective columns of $\boldsymbol{B}(\omega_i)$ to be mapped. Relating equation 2.5 to equation 2.11 for the $P = 1$ case, we see that $T_{st}(\omega_i;\boldsymbol{B}(\omega_i)) = \boldsymbol{E}^{-1}(\omega_i;\beta)$, $\boldsymbol{B}(\omega_i) = \boldsymbol{e}(\omega_i;\boldsymbol{\beta})$, and $\boldsymbol{G} = \mathbf{1}$. However, P can be greater than 1 and it is beneficial to have P as large as possible to decrease the number of matrix inversions. In fact, if we choose $P = M$ we get

$$T_{st}(\omega_i;\boldsymbol{B}(\omega_i)) = \boldsymbol{G}\boldsymbol{B}^{-1}(\omega_i) \tag{2.12}$$

if $\boldsymbol{B}(\omega_i)$ is full rank. Note that when implementing equation 2.12, we might encounter numerical difficulties if our presteering directions are spatially very close since the inversion of $\boldsymbol{B}(\omega_i)$ might become unstable, i.e., $\boldsymbol{B}(\omega_i)$ might be *numerically singular.*

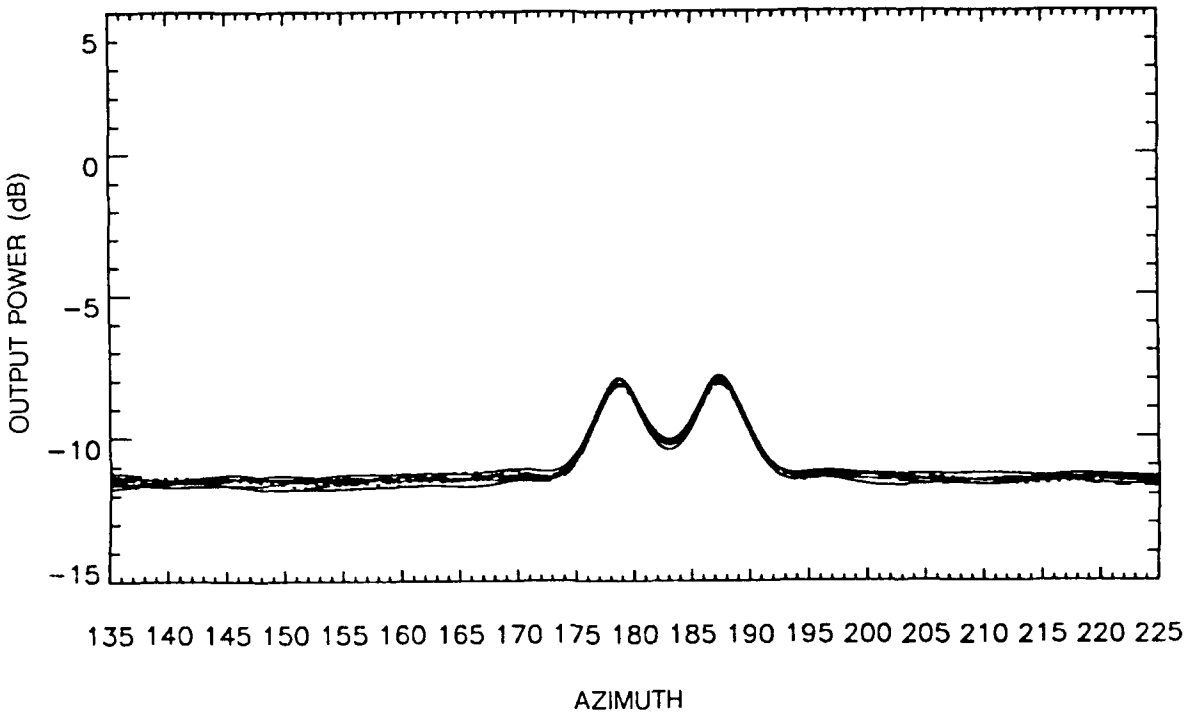

Figure 2-9. Incoherent MVDR processor results for two perfectly correlated sources.

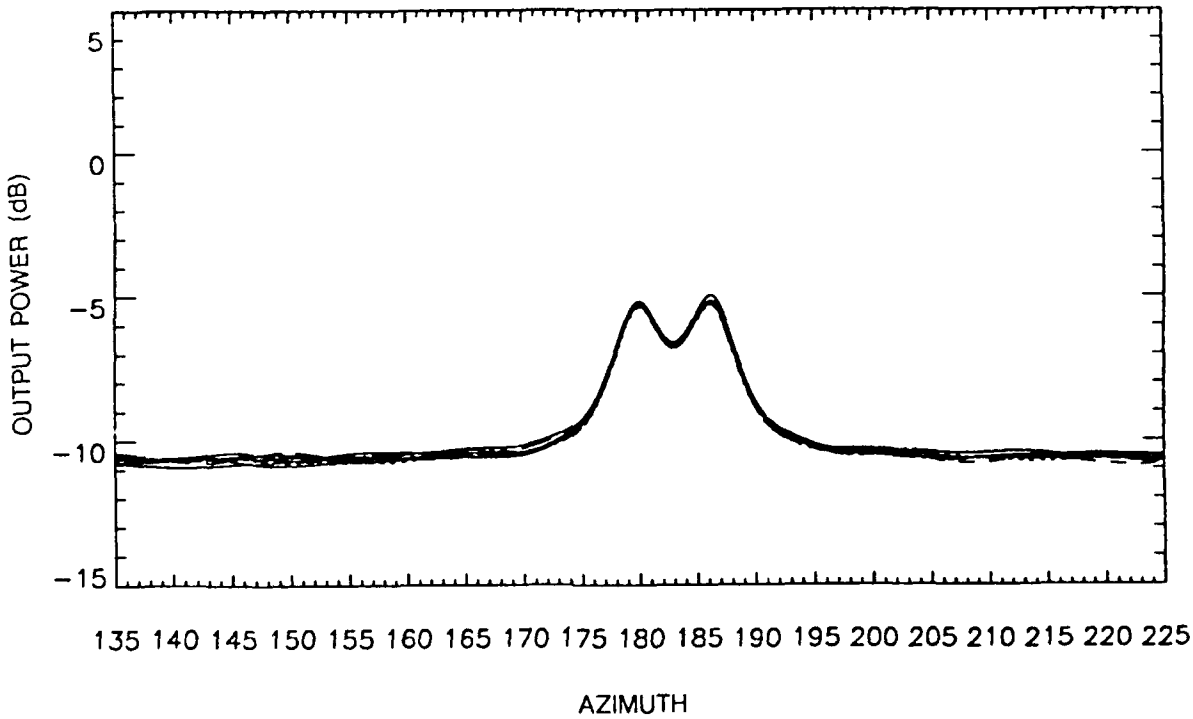

Figure 2-10. Coherent MVDR processor results for two perfectly correlated sources.

If $1 < P < M$ we could use the pseudo-inverse of $\boldsymbol{B}(\omega_i)$ to calculate $T_{st}(\omega_i; \boldsymbol{B}(\omega_i))$. If $P > M$ there is no solution to this overdetermined system of equations. However, we might still obtain adequate presteering if we use the least squares solution to the problem as

$$T_{st}(\omega_i; \boldsymbol{B}(\omega_i)) = \boldsymbol{G}\boldsymbol{B}^H(\omega_i)[\boldsymbol{B}(\omega_i)\boldsymbol{B}^H(\omega_i)]^{-1} \quad . \tag{2.13}$$

How well we can presteer and coherently add across frequency if $P >> M$ is unclear.

Now, using equation 2.12 or equation 2.13 for our steering matrix, we get the multiply-steered, coherent CSDM

$$\boldsymbol{R}_c(\boldsymbol{B}) = \sum_i \boldsymbol{T}_{st}^H(\omega_i; \boldsymbol{B}(\omega_i))\boldsymbol{R}(\omega_i)\boldsymbol{T}_{st}(\omega_i; \boldsymbol{B}(\omega_i)) \quad . \tag{2.14}$$

Then,

$$P_{c\_mvdr}(\boldsymbol{g}_k) = \frac{1}{\boldsymbol{g}_k^H \boldsymbol{R}_c^{-1}(\boldsymbol{B})\boldsymbol{g}_k} \quad , \tag{2.15}$$

where $\boldsymbol{g}_k$ is the k^{th} column of $\boldsymbol{G}$. So for each matrix inverse we can steer over P directions where $1 \leq k \leq P$. The multiply-steered coherent MVDR method is then P times less computationally intensive than the technique of equation 2.9. So, generally, the larger the number of sensors, the more directions we can presteer towards in *one* $\boldsymbol{R}_c(\boldsymbol{\beta})$. The computational overhead of coherent MVDR might not be severe for large arrays.

We have complete freedom in choosing $\boldsymbol{G}$. A convenient form would be an orthogonal or orthonormal matrix if $P < M$. Then if $\boldsymbol{T}_{st}(\omega_i; \boldsymbol{B}(\omega_i))$ contains *more* than one source signal vector from $\boldsymbol{A}(\omega_i)$ of equation 2.1, $\boldsymbol{R}_c(\boldsymbol{\beta})$ would contain orthogonal components. This in turn could enhance nulling performance. We could also use a $\boldsymbol{G}$ matrix with M orthogonal basis columns and $P - M$ columns spanned by the basis vectors if $P > M$.

We could also use multiple presteering for coherent conventional processing. Then multiply-steered coherent conventional processing would *not* equal incoherent conventional results. It is unclear what the performance differences would be between single and multiple direction coherent MVDR and conventional processing. Certainly, presteering and coherently summing two or more signal vectors in one coherent CSDM will affect broadband array processing performance.

2.3.4 Coherent Processing Applied to MUSIC

We have confined our attention to coherent MVDR mainly for instructional purposes. However, it is a simple matter to use the coherent CSDM $\boldsymbol{R}_c(\boldsymbol{\beta})$ from section 2.3 in the MUSIC algorithm. If we compute the eigen decomposition of $\boldsymbol{R}_c(\boldsymbol{\beta})$ as

$$\boldsymbol{R}_c(\boldsymbol{\beta}) = \sum_{i=1}^{M} \lambda_{ci} \boldsymbol{v}_{ci} \boldsymbol{v}_{ci}^H \quad , \tag{2.16}$$

where v_{ci} are the eigenvectors and λ_{ci} the associated eigenvalues with $\lambda_{c1} \geq \lambda_{c2} \geq \ldots \geq \lambda_{cM}$, then the well-known MUSIC algorithm produces

$$P_{c\_music}(\boldsymbol{\beta}) = \frac{1}{\sum_{i=1}^{M-n} 1^T v_{ci} v_{ci}^H 1}, \tag{2.17}$$

where n is the user-specified order. If we were able to model the noise matrix component of $\boldsymbol{R}_c(\boldsymbol{\beta})$, we could also implement a generalized MUSIC algorithm as in Wang and Kaveh (1985). For multiply-steered CSDMs we get

$$P_{c\_music}(\boldsymbol{g}_k) = \frac{1}{\sum_{i=1}^{M-n} g_k^H v_{ci} v_{ci}^H g_k}. \tag{2.18}$$

Unfortunately, order selection in MUSIC can be quite problematic.

2.3.4.1 Simulations

We examine the narrowband "CSDMs" constructed from three independent FFTs per matrix used to produce the results of figure 2-8. Figures 2-11, 2-12, and 2-13 are the MUSIC results from equation 2.17 for orders one, two, and three respectively. Since we are incoherently summing signal components across frequency in $\boldsymbol{R}_c(\boldsymbol{\beta})$ when we are not steered towards a component, one might assume an order of one would be appropriate because there should be at most one dominant correlated component in $\boldsymbol{R}_c(\boldsymbol{\beta})$. Figure 2-11 indicates that this is not the case and an order of two is still required since spectral averaging is not sufficient to completely "whiten" a correlated component. Comparison of figure 2-12 with figure 2-8 reveals that coherent MUSIC offers greater resolution in the signal directions and, interestingly, less variance in the side regions.

2.4 TIME-DOMAIN ARRAY PROCESSING

Methods have been proposed recently that localize acoustic sources using time-domain techniques (Clay, 1987; Li and Clay, 1987; Clay and Li, 1988; and Hodgkiss and Brienzo, 1990). These methods use matched-filter or inverse-filter approaches to essentially remove, to a certain extent, the propagation environment from the signals received at each of the sensors and then to use various processing methods such as estimating correlation statistics to localize sources.

Figure 2-14 is a generalized diagram of these techniques. $y_i(t)$ represents the data received at the i^{th} sensor (see figure 1-1), and $\hat{h}(t;\boldsymbol{\beta}_{si})$ is the matched or inverse filter impulse response for the i^{th} sensor focused or steered to a spatial location specified by $\boldsymbol{\beta}_{si}$. We have also included a time-varying steering filter $\hat{h}_t(t;\boldsymbol{\beta}_{sit})$ in the diagram to indicate the possible extension to a spatial and/or temporal nonstationary environment.

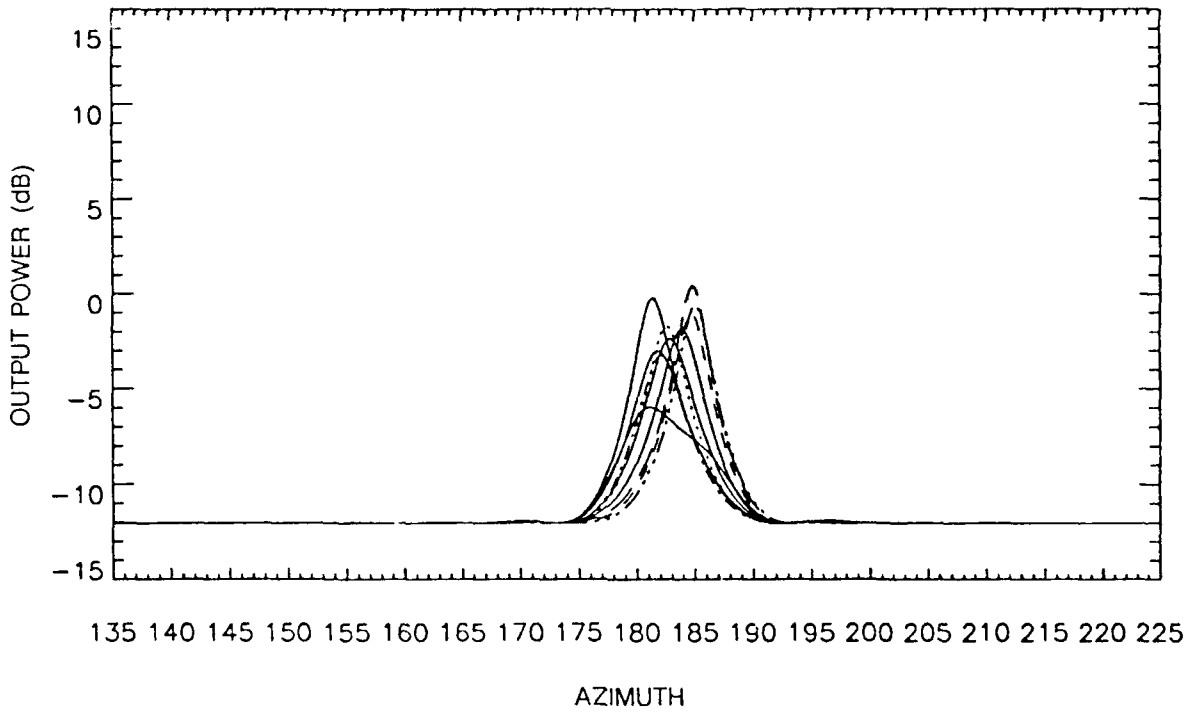

Figure 2-11. Coherent MUSIC results with n = 1 and three independent FFTs per "CSDM."

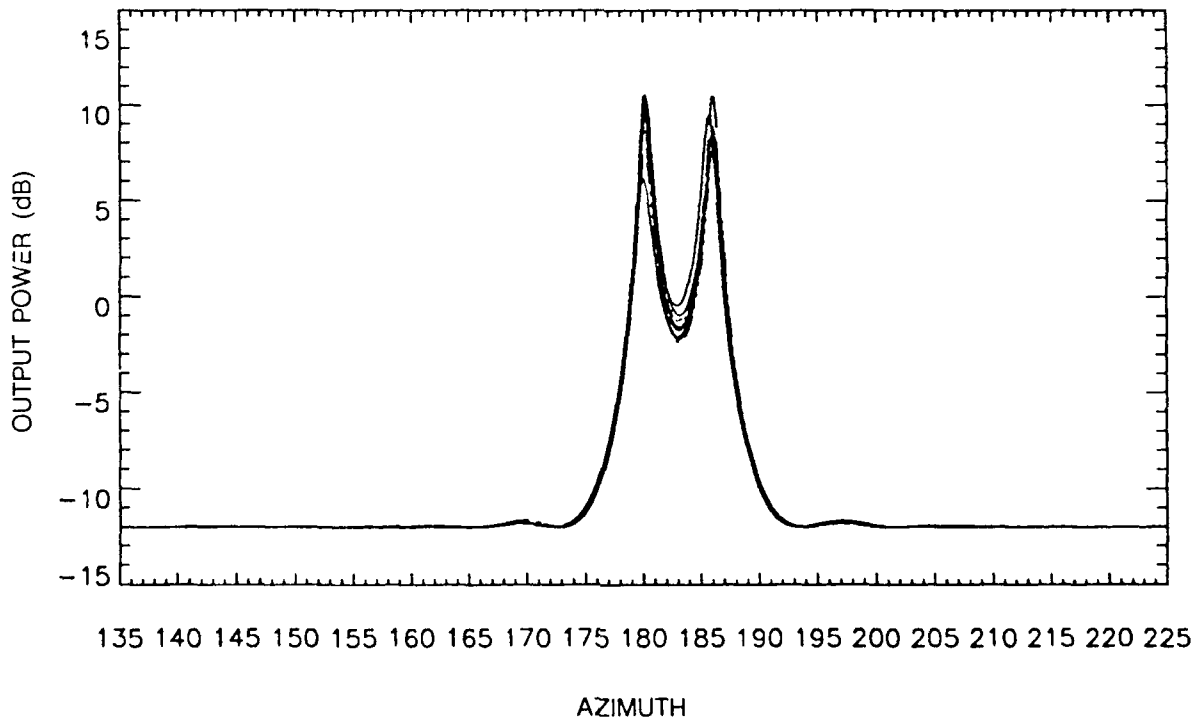

Figure 2-12. Coherent MUSIC results with n = 2 and three independent FFTs per "CSDM."

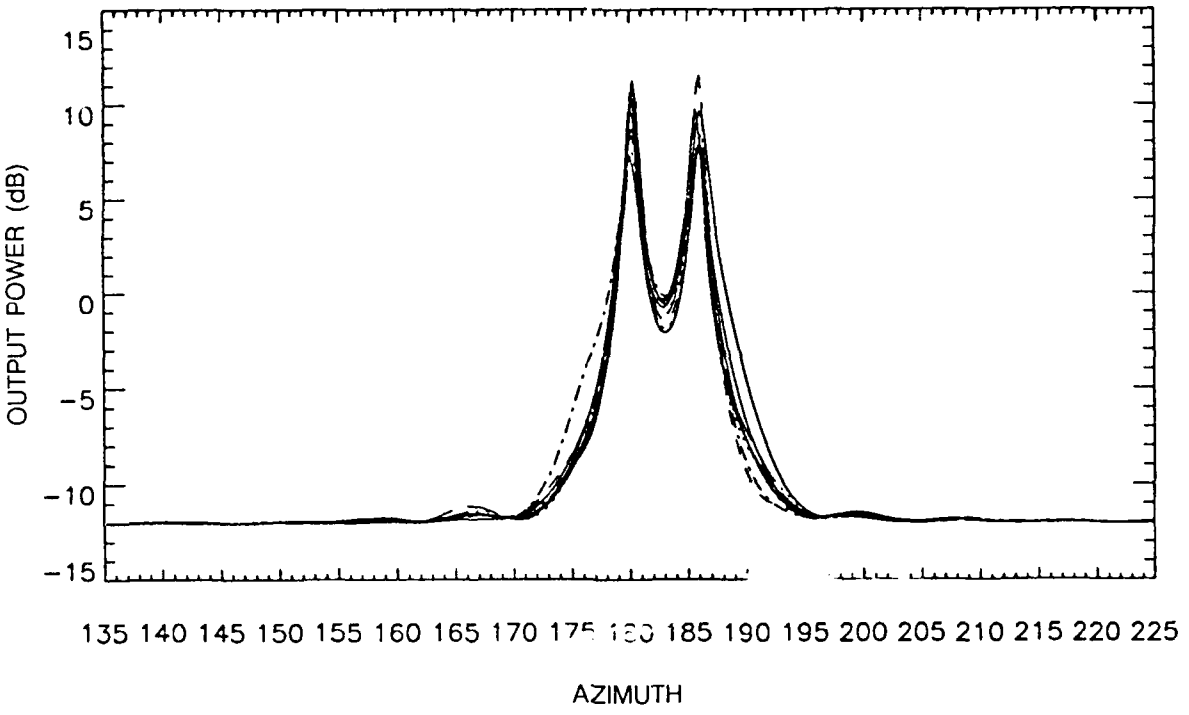

Figure 2-13. Coherent MUSIC results with n = 3 and three independent FFTs per "CSDM."

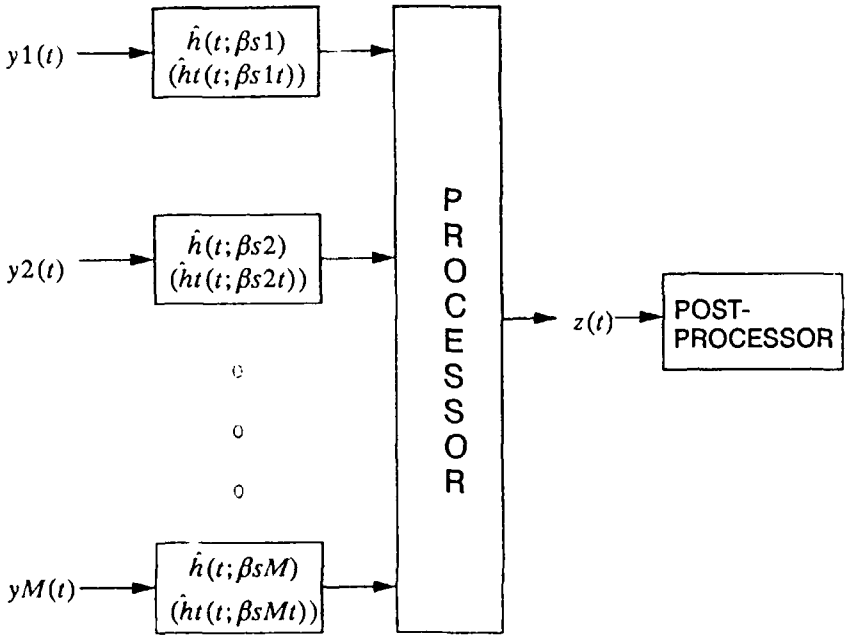

Figure 2-14. Generalized time-domain array processor diagram.

To compute the focusing filter, the channel impulse response is first required. It can be estimated analytically with time-domain propagation models or via Fourier synthesis using frequency-domain propagation techniques (Hodgkiss and Brienzo, 1990), or, if possible, determined experimentally using an impulsive source (Clay, 1987; Li and Clay, 1987; Clay and Li, 1988). The outputs of these filters are then processed using simple summing for conventional processing as in Hodgkiss and Brienzo (1990), or cross correlating between sensors as in Clay (1987), Li and Clay (1987), and Clay and Li (1988). Future work could include a tapped-delay-line-based MVDR technique as in Frost (1972), which is also useful in highly nonstationary environments. In fact there are similarities between a Frost-based, time-domain matched-field MVDR processor and the coherent MVDR technique. The output of the processor can then be sent to a postprocessor that might spectrally decompose the data, compute energy (Hodgkiss and Brienzo, 1990), or do spectral peak detection (Clay, 1987; Li and Clay, 1987; Clay and Li, 1988).

2.4.1 Matched-Filter Method

In the matched-filter approach, each of the steering filters of figure 2-11 has an impulse response that is the time reverse of the respective channel impulse response with an associated time shift to ensure causality. The data received at each sensor are convolved with the impulse response of the matched filter. While this method will not entirely remove the environment from the signal, the more complicated the environment (the longer the channel impulse response), the better the performance of this approach (Clay, 1987). It is also simple and very robust.

2.4.2 Inverse-Filter Method

A time-domain analogue to the frequency-domain techniques of equations 1.3 and 1.4 is the inverse-filter method. Here the steering filters are computed such that

$$\hat{h}(t;\boldsymbol{\beta}_{si}) * h(t;\boldsymbol{\beta}_{si}) = \delta(t), \tag{2.19}$$

where * denotes linear convolution and $\delta(t)$ is the Dirac delta function. So if we steer directly at a signal $s(t)$ with power spectral density $\sigma_s^2(\omega)$, the power spectral density due to the signal at *each* focusing filter output also will be $\sigma_s^2(\omega)$.

As noted in Clay and Li (1988) for the discrete-time case, care must be taken if the channel transfer function is *not* minimum phase, i.e., the zeros of the Laplace transform of $h(t;\boldsymbol{\beta}_{si})$ are not all in the left half of the complex plane, or, for the discrete-time case, the zeros of the z-transform of $h(n;\boldsymbol{\beta}_{si})$are not all inside the unit circle. The causal inverse filter would then be unstable, i.e., the impulse response would not be absolutely integrable (summable). Standard zero reflection and appropriate time-shifting can solve this problem, e.g., see Oppenheim and Schafer (1989) for the discrete-time case. This

technique obviously requires more processing than the matched-filter method. However, if the channel transfer function has a zero on the imaginary axis (the unit circle for the discrete-time case), no stable inverse filter can be found. An interesting topic would be to determine analytically the conditions, e.g., the boundary conditions on the wave equation, that result in a minimum-phase channel.

We can now recognize a benefit of the frequency-domain coherent MVDR algorithm over a time-domain, Frost-based MVDR method. Since we are interested only in calculating a particular *frequency response* in equation 2.7 over the ω_i of interest rather than in calculating an impulse response, we do not have to worry about causality or stability of the inverse filter.

REFERENCES

Blachman, N. M. 1957. "On Fourier Series for Gaussian Noise," *Inf. Control* 1, pp. 56–63.

Buckley, K. M. 1987. "Spatial/Spectral Filtering with Linearly Constrained Minimum Variance Beamformers," *IEEE Trans., Acoust. Speech, Signal Processing*, vol. ASSP-35, no. 3, pp. 249–266 (March).

Buckley, K. M., and L. J. Griffiths. 1988. "Broadband Signal-Subspace Spatial-Spectrum (BASS-ALE) Estimation," *IEEE Trans., Acoust. Speech, Signal Processing*, vol. 36, no. 7, pp. 953–964 (July).

Chen, C. T. 1984. *Linear System Theory and Design*. Holt, Rinehart and Winston, New York, NY, chap. 3.

Clay, C. S. 1987. "Optimum Time Domain Signal Transmission and Source Location in a Waveguide," *J. Acoust. Soc. Am.*, vol. 81, no. 3, pp. 660–664 (March).

Clay, C. S., and S. Li. 1988. "Time Domain Signal Transmission and Source Location in a Waveguide: Matched Filter and Deconvolution Experiments," *J. Acoust. Soc. Am.*, vol. 83, no. 4, pp. 1377–1383 (April).

Dudgeon, D. E., and R. M. Mersereau. 1984. *Multidimensional Digital Signal Processing*. Prentice-Hall, Inc., Englewood Cliffs, NJ, chap. 6.

Frost, O. L. 1972. "An Algorithm for Linearly Constrained Adaptive Array Processing," *Proceedings of the IEEE*, vol. 60. pp. 926–935 (Aug).

Gerlach, A. A. 1978. "Motion Induced Coherence Degradation in Passive Systems," *IEEE Trans., Acoust. Speech, Signal Processing*, vol. ASSP-26, no. 1, pp. 1–15 (Feb).

Giannella, F. A., and P. M. Schultheiss. 1990. "Efficient Location of Closely Spaced Wide-Band Sources," in *Proc. ICASSP-90*, Albuquerque, NM, pp. 2915–2918 (April).

Gingras, D. F. 1989. "Methods for Predicting the Sensitivity of Matched-Field Processors to Mismatch," *J. Acoust. Soc. Am.*, vol. 86, no. 5, pp. 1940–1949 (Nov).

Hodgkiss, W. S. 1979. "Adaptive Array Processing: Time vs. Frequency Domain," in *Proc. ICASSP-79*, Washington, DC, pp. 282–285 (April).

Hodgkiss, W. S., and R. K. Brienzo. 1990. "Broadband Matched Field Processing," in *Proc. ICASSP-90*, Albuquerque, NM, pp. 2743–2746 (April).

Hodgkiss, W. S., and L. W. Nolte. 1976. "Covariance Between Fourier Coefficients Representing the Time Waveforms Observed From an Array of Sensors," *J. Acoust. Soc. Am.*, vol. 59, no. 3, pp. 582–590 (March).

Hudson, J. E. 1981. *Adaptive Array Principles*. The Institution of Electrical Engineers, London, NY, pp. 27–28.

Johnson, D. H. 1982. "The Application of Spectral Estimation Methods to Bearing Estimation Problems," *Proceedings of the IEEE*, vol. 70, no. 9, pp. 1018–1028 (Sep).

Kennedy, R. S., and I. L. Lebow. 1964. "Signal Design for Dispersive Channels," *IEEE Spectrum*, pp. 231–237 (March).

Kitagawa, G., and W. Gersch. 1985. "A Smoothness Priors Time-Varying AR Coefficient Modeling of Nonstationary Covariance Time Series," *IEEE Trans., Automat. Contr.*, vol. AC-30, no. 1, pp. 48–56 (Jan).

Knight, W. C., R. G. Pridham, and S. M. Kay. 1981. "Digital Signal Processing for Sonar," *Proceedings of the IEEE*, vol. 69, no. 11, pp. 1451–1507 (Nov).

Krolik, J., and D. Swingler. 1989. "Multiple Broad-Band Source Location Using Steered Covariance Matrices," *IEEE Trans., Acoust. Speech, Signal Processing*, vol. 37, no. 10, pp. 1481–1494 (Oct).

Li, S., and C. S. Clay. 1987. "Optimum Time Domain Signal Transmission and Source Location in a Waveguide: Experiments in an Ideal Wedge Waveguide," *J. Acoust. Soc. Am.*, vol. 82, no. 4, pp. 1409–1417 (Oct).

Morgan, D. R., and T. M. Smith. 1990. "Coherence Effects on the Detection Performance of Quadratic Processors, with Applications to Large Array Matched-Field Beamforming," *J. Acoust. Soc. Am.*, vol. 87, no. 2, pp. 737–747 (Feb).

Nawab, S. H., F. U. Dowla, and R. T. Lacoss. 1985. "Direction Determination of Wideband Signals," *IEEE Trans., Acoust. Speech, Signal Processing*, vol. ASSP-33, no. 4, pp. 1114–1122 (Oct).

Oppenheim, A. V., and R. W. Schafer. 1989. *Discrete-Time Signal Processing*. Prentice-Hall, Inc., Englewood Cliffs, NJ, pp. 209–211.

Papoulis, A. 1984. *Probability, Random Variables, and Stochastic Processes*. McGraw-Hill, New York, NY, pp. 306–307.

Patzewitsch, J. T., and M. D. Srinath. 1978. "Near-Field Performance of Passive Coherence Processing Sonars," *IEEE Trans., Acoust. Speech, Signal Processing*, vol. ASSP-27, no. 6, pp. 573–582 (Feb).

Thomas, J. B. 1984. *An Introduction to Applied Probability and Random Processes*. Robert E. Krieger Publishing Co., Malabar FL, pp. 229–230.

Tolstoy, A., and M. B. Porter. 1986. "Broadband Acoustic Source Localization in a Deep Water Pacific Environment," unpublished NRL report.

Wang, H., and M. Kaveh. 1985. "Coherent Signal-Subspace Processing for the Detection and Estimation of Angles of Arrival of Multiple Wide-Band Sources," *IEEE Trans., Acoust. Speech, Signal Processing*, vol. ASSP-33, no. 4, pp. 823–831 (Aug).

Wax, M., T. Shan, and T. Kailath. 1984. "Spatio-Temporal Spectral Analysis by Eigenstructure Methods," *IEEE Trans., Acoust. Speech, Signal Processing*, vol. ASSP-32, no. 4, pp. 817–827 (Aug).

Weinstein, E. 1978. "Estimation of Trajectory Parameters From Passive Array Measurements," Ph.D. dissertation, Yale University, New Haven, CT.

REPORT DOCUMENTATION PAGE

Form Approved
OMB No. 0704-0188

1 AGENCY USE ONLY *(Leave blank)*	2 REPORT DATE	3 REPORT TYPE AND DATES COVERED
	April 1991	Final

4 TITLE AND SUBTITLE
ISSUES AND METHODS OF BROADBAND ARRAY PROCESSING

5 FUNDING NUMBERS
0602314N
RJ14C32
SUB8
DN 308105

6 AUTHOR(S)
M. Reuter

7 PERFORMING ORGANIZATION NAME(S) AND ADDRESS(ES)
Naval Ocean Systems Center
San Diego, CA 92152–5000

8 PERFORMING ORGANIZATION REPORT NUMBER
NOSC TD 2086

9 SPONSORING/MONITORING AGENCY NAME(S) AND ADDRESS(ES)
Naval Ocean Systems Center
San Diego, CA 92152–5000

10 SPONSORING/MONITORING AGENCY REPORT NUMBER

11 SUPPLEMENTARY NOTES

12a DISTRIBUTION/AVAILABILITY STATEMENT
Approved for public release; distribution is unlimited.

12b DISTRIBUTION CODE

13 ABSTRACT *(Maximum 200 words)*

This document contains observations concerning the analysis of broadband processes as applied to passive spatial array processing. The analysis is intended to be applicable to general acoustic propagation environments.

In section 1.0, we use a linear systems model of the propagation environment in our analysis of the spatial/spectral estimation problem. We show how this view also might be used in the moving source problem. We also briefly discuss correlations between Fourier coefficients at different frequencies.

In section 2.0, we look at approaches to broadband array processing that take advantage of the frequency extent of the source process in estimating the spatial spectrum.

14 SUBJECT TERMS
cross spectral density matrix (CSDM)
discrete Fourier transform

15 NUMBER OF PAGES
36

16 PRICE CODE

17 SECURITY CLASSIFICATION OF REPORT	18 SECURITY CLASSIFICATION OF THIS PAGE	19 SECURITY CLASSIFICATION OF ABSTRACT	20 LIMITATION OF ABSTRACT
UNCLASSIFIED	UNCLASSIFIED	UNCLASSIFIED	SAME AS REPORT

21a. NAME OF RESPONSIBLE INDIVIDUAL	21b. TELEPHONE *(Include Area Code)*	21c. OFFICE SYMBOL
M. Reuter	(619) 553-2045	Code 733

INITIAL DISTRIBUTION

Code 0012	Patent Counsel	(1)
Code 0144	R. November	(1)
Code 705	D. Hanna	(1)
Code 7304	G. Mohnkern	(1)
Code 732	C. Persons	(1)
Code 733	D. Barbour	(1)
Code 733	M. Reuter	(5)
Code 952B	J. Puleo	(1)
Code 961	Archive/Stock	(6)
Code 964B	Library	(3)

Defense Technical Information Center
Alexandria, VA 22304-6145 (4)

NOSC Liaison Office
Washington, DC 20363-5100 (1)

Center for Naval Analyses
Alexandria, VA 22302-0268 (1)